

# Molecular-level analysis of the serum antibody repertoire in young adults before and after seasonal influenza vaccination

Jiwon Lee<sup>1</sup>, Daniel R Boutz<sup>2</sup>, Veronika Chromikova<sup>3</sup>, M Gordon Joyce<sup>4</sup>, Christopher Vollmers<sup>5</sup>, Kwanyee Leung<sup>4</sup>, Andrew P Horton<sup>2</sup>, Brandon J DeKosky<sup>1,15</sup>, Chang-Han Lee<sup>1</sup>, Jason J Lavinder<sup>1</sup>, Ellen M Murrin<sup>1</sup>, Constantine Chrysostomou<sup>1</sup>, Kam Hon Hoi<sup>6,15</sup>, Yaroslav Tsybovsky<sup>7</sup>, Paul V Thomas<sup>4</sup>, Aliaksandr Druz<sup>4</sup>, Baoshan Zhang<sup>4</sup>, Yi Zhang<sup>4</sup>, Lingshu Wang<sup>4</sup>, Wing-Pui Kong<sup>4</sup>, Daechan Park<sup>1</sup>, Lyubov I Popova<sup>8,15</sup>, Cornelia L Dekker<sup>9</sup>, Mark M Davis<sup>10,11</sup>, Chalise E Carter<sup>12</sup>, Ted M Ross<sup>12</sup>, Andrew D Ellington<sup>2,13</sup>, Patrick C Wilson<sup>8</sup>, Edward M Marcotte<sup>2,13</sup>, John R Mascola<sup>4</sup>, Gregory C Ippolito<sup>13</sup>, Florian Krammer<sup>3</sup>, Stephen R Quake<sup>5,10,14</sup>, Peter D Kwong<sup>4</sup> & George Georgiou<sup>1,2,6,13</sup>

Molecular understanding of serological immunity to influenza has been confounded by the complexity of the polyclonal antibody response in humans. Here we used high-resolution proteomics analysis of immunoglobulin (referred to as Ig-seq) coupled with high-throughput sequencing of transcripts encoding B cell receptors (BCR-seq) to quantitatively determine the antibody repertoire at the individual clonotype level in the sera of young adults before and after vaccination with trivalent seasonal influenza vaccine. The serum repertoire comprised between 40 and 147 clonotypes that were specific to each of the three monovalent components of the trivalent influenza vaccine, with boosted pre-existing clonotypes accounting for ~60% of the response. An unexpectedly high fraction of serum antibodies recognized both the H1 and H3 monovalent vaccines. Recombinant versions of these H1 + H3 cross-reactive antibodies showed broad binding to hemagglutinins (HAs) from previously circulating virus strains; several of these antibodies, which were prevalent in the serum of multiple donors, recognized the same conserved epitope in the HA head domain. Although the HA-head-specific H1 + H3 antibodies did not show neutralization activity *in vitro*, they protected mice against infection with the H1N1 and H3N2 virus strains when administered before or after challenge. Collectively, our data reveal unanticipated insights regarding the serological response to influenza vaccination and raise questions about the added benefits of using a quadrivalent vaccine instead of a trivalent vaccine.

Influenza infections cause over 5 million cases of severe illness, resulting in approximately half a million deaths globally, every year and pose a threat of another pandemic<sup>1,2</sup>. The HA surface glycoprotein is the main antigenic determinant of the influenza virus, and neutralizing antibodies that bind to HA are known to confer protective immunity<sup>3,4</sup>. The seasonal trivalent inactivated influenza vaccine (IIV3) that is currently in use contains HA from two influenza A strains (H1N1 and H3N2) and one influenza B strain (either the Yamagata or Victoria lineage). However, it has been estimated that IIV3 confers

protection in only about 60% of young adults, and efficacy can be substantially lower for at-risk groups such as infants and the elderly<sup>5,6</sup>. For this reason, improved vaccination strategies are needed.

Currently, hemagglutination inhibition (HAI) titers, which measure the amounts of antibodies that inhibit viral infection through preventing HA binding to its target cell receptors, are used as the main metric of vaccine efficacy<sup>7,8</sup>. However, HAI assays only inform on antibodies that disrupt binding between the receptor-binding site (RBS) of HA and its receptor. Influenza can also be neutralized

<sup>1</sup>Department of Chemical Engineering, University of Texas at Austin, Austin, Texas, USA. <sup>2</sup>Center for Systems and Synthetic Biology, University of Texas at Austin, Austin, Texas, USA. <sup>3</sup>Department of Microbiology, Icahn School of Medicine at Mount Sinai, New York, New York, USA. <sup>4</sup>Vaccine Research Center, National Institute of Allergy and Infectious Diseases, US National Institutes of Health, Bethesda, Maryland, USA. <sup>5</sup>Department of Bioengineering, Stanford University, Stanford, California, USA. <sup>6</sup>Department of Biomedical Engineering, University of Texas at Austin, Austin, Texas, USA. <sup>7</sup>Electron Microscopy Laboratory, Cancer Research Technology Program, Leidos Biomedical Research, Inc., Frederick National Laboratory for Cancer Research, Frederick, Maryland, USA. <sup>8</sup>Department of Medicine, Section of Rheumatology, Gwen Knapp Center for Lupus and Immunology Research, University of Chicago, Chicago, Illinois, USA. <sup>9</sup>Department of Pediatrics, Stanford University, Stanford, California, USA. <sup>10</sup>Howard Hughes Medical Institute, Stanford University, Stanford, California, USA. <sup>11</sup>Department of Microbiology and Immunology, Stanford University, Stanford, California, USA. <sup>12</sup>Center for Vaccines and Immunology, Department of Infectious Diseases, University of Georgia, Athens, Georgia, USA. <sup>13</sup>Department of Molecular Biosciences, University of Texas at Austin, Austin, Texas, USA. <sup>14</sup>Department of Applied Physics, Stanford University, Stanford, California, USA. <sup>15</sup>Present addresses: Vaccine Research Center, National Institute of Allergy and Infectious Diseases, US National Institutes of Health, Bethesda, Maryland, USA (B.J.D.); Antibody Engineering Department, Genentech, Inc., South San Francisco, California, USA (K.H.H.); Division of Infectious Diseases, SRI International, Harrisonburg, Virginia, USA (L.I.P.). Correspondence should be addressed to G.G. (gg@che.utexas.edu).

Received 10 July; accepted 4 October; published online 7 November 2016; doi:10.1038/nm.4224

by other mechanisms, most notably by antibodies that bind to the conserved stem region of HA and interfere with fusion between the virus and the host endosomal membranes after endocytosis of the virus<sup>9–12</sup>. Stem-binding, broadly neutralizing antibodies (bNAbs) are rarely elicited after seasonal vaccination<sup>13–15</sup>, although they have been detected at increased frequencies in individuals who were infected or vaccinated with divergent strains, such as H5N1 or the 2009 pandemic H1N1 strain<sup>12,16–19</sup>. In addition, it should be noted that *in vitro* neutralization activity does not always correlate with *in vivo* protection in mouse models<sup>11,20,21</sup> that are widely used to evaluate antibody-mediated protection against challenge with live influenza virus<sup>22,23</sup>.

Over the past few years, cloning and characterization of antibodies from peripheral blood B cells has enhanced our understanding of antibody-mediated protection to influenza<sup>10,11,13,24–26</sup>. More recently, high-throughput sequencing of transcripts encoding heavy chain variable ( $V_H$ ) regions from B cells in peripheral blood has also provided new insights about features of the influenza vaccine response<sup>27–31</sup>. Nevertheless, it is antibodies circulating in serum, not immunoglobulin receptors on B cells, that directly mediate protection against viral infection. For that reason, bulk serological metrics, including ELISA and neutralization titers to viral strains, have also been used to understand the response to vaccination or infection. However, neither investigation of peripheral B cells nor bulk serological assays provide information regarding the sequence, relative concentrations, temporal dynamics and functions of the individual monoclonal antibodies that comprise the polyclonal anti-influenza serum repertoire. Here we study the serum antibody repertoire at a molecular level to determine the extent to which seasonal influenza vaccination either boosts levels of pre-existing serum antibodies or elicits new antibodies, the influenza-binding breadth, protection potencies and mechanisms of action of vaccine-boosted and vaccine-elicited antibodies, how clonal diversity of the serum repertoire is affected by immunization and how it relates to the overall ELISA titer, and finally, the persistence of individual clones over time in the serum.

## RESULTS

### The serological repertoire to IIV3

We previously developed a proteomics-based pipeline for the identification and semiquantitative determination of the antigen-specific antibodies in human serum<sup>32–34</sup>. By using this method, we delineated the composition and relative quantities of the antibody clonotypes comprising the serum IgG repertoire before (pre-) and after (post-) vaccination (days 0, 28 and 180) in four human donors who were immunized with the 2011–2012 IIV3 vaccine (**Fig. 1a** and **Supplementary Table 1**). Briefly, serum IgG specific for each of the three vaccine strains was purified by three separate affinity chromatography columns, each using one of the monovalent inactivated vaccine components (IIV1) that comprise the IIV3 (A/California/07/2009 X-179A, A/Victoria/210/2009 X-187 and B/Brisbane/60/2008; abbreviated as ‘H1 A/CA09’, ‘H3 A/VI09’ and ‘Vic B/BR08’, respectively). The influenza-specific antibodies in the affinity chromatography elution fraction were trypsinized and analyzed by high-resolution liquid chromatography coupled to tandem mass spectrometry (LC–MS/MS). In total, analysis of the serological repertoire for all of the time points and donors required 240 runs and >1,200 h of LC–MS/MS time, with collection of >7,000,000 mass spectra.

Antibodies that share sequence similarity in the heavy chain complementarity-determining region 3 (CDR-H3) and have the same

binding specificity belong to a particular clonotype and are likely to recognize the same epitope. For our analyses, we identified high-confidence CDR-H3 peptides and grouped the peptides belonging to the same clonotype together. The corresponding LC peak intensities were used for relative quantification of the antibody clonotypes<sup>35</sup>. An estimated >80% of the CDR-H3 peptides within a sample are typically identified in this manner (detection limit around 0.4 ng/ml), and quantification calibrations using isobaric peptide spike-ins showed that peak intensities correlate well with absolute peptide concentrations<sup>36</sup>. Accordingly, our proteomic methodology enabled us to quantify changes in the abundance of different antibody clonotypes among the serum repertoire of antibodies that bind to each IIV1.

For each time point, the antibody repertoire composition and relative quantities at the clonotypic level were plotted as a histogram, with each bar representing an individual clonotype and the  $y$  axis showing its relative abundance (**Fig. 1b**). We defined antibody clonotypes present in both the pre-vaccination repertoire (day 0) and the post-vaccination repertoire (day 28 and/or day 180) as ‘pre-existing’, and clonotypes observed exclusively in the post-vaccination repertoire (not at day 0) as ‘vaccine-elicited’. The term ‘vaccine-elicited antibodies’ refers only to the fact that these antibodies become detectable in the serum after vaccination and should not be interpreted in B cell ontogeny terms (i.e., whether they arise from stimulated naive or memory B cells). The temporal dynamics of the serum repertoire to each IIV1 at days 0, 28 and 180 are represented as heat maps, with color intensity reflecting relative amount of the respective clonotype (**Fig. 1c** and **Supplementary Fig. 1**). The comparison of pre-existing and vaccine-elicited antibodies revealed that in the four donors we analyzed, on average pre-existing antibody clonotypes comprised 61.2% and 65.4% of the HA-binding repertoire in day 28 and day 180 sera, respectively (**Fig. 1d**). Thus, the post-vaccination response is dominated by pre-existing serum antibodies.

Inspection of the serological repertoires for all of the donors also revealed several additional insights. First, the number of distinct antibody clonotypes specific for each IIV1 ranged from as low as 6 at day 0 to between 40 and 147 at day 28 (**Supplementary Table 2**), revealing that the influenza-specific repertoire is highly restricted and oligoclonal. Second, the serological repertoire is highly polarized, and on average, the top 6% of the most abundant clonotypes after vaccination account for more than 60% of the entire repertoire (**Supplementary Table 3**). This polarization effect is also evident in the pre-vaccination serum IgG repertoires (top 12% antibody clonotypes constituting >60% of the repertoire). Third, the number of antibody clonotypes in the serum repertoire specific for a particular IIV1 correlates with the respective serum titer (Spearman correlation = 0.82,  $P < 0.0001$ ; **Fig. 1e** and **Supplementary Table 4**). Fourth, the frequency of vaccine-elicited antibody clonotypes shows an inverse correlation with the serum titer before vaccination (Spearman correlation =  $-0.82$ ,  $P = 0.0010$ ; **Fig. 1f**). In other words, individuals with a lower serum titer before vaccination, and therefore a repertoire comprising fewer antibody clonotypes, produce a greater number of vaccine-elicited antibody clonotypes. These data are consistent with a model (**Supplementary Fig. 2**) in which the greater the number of pre-existing clonotypes (reflected as a higher pre-vaccination serum titer), the greater the number of antigenic epitopes that are bound by circulating antibodies resulting in a blockade of antigenic sites (or possibly, more effective clearance owing to the formation of HA immune complexes decorated with a larger number of antibodies), thereby reducing the magnitude and diversification of the B cell response<sup>37,38</sup>.

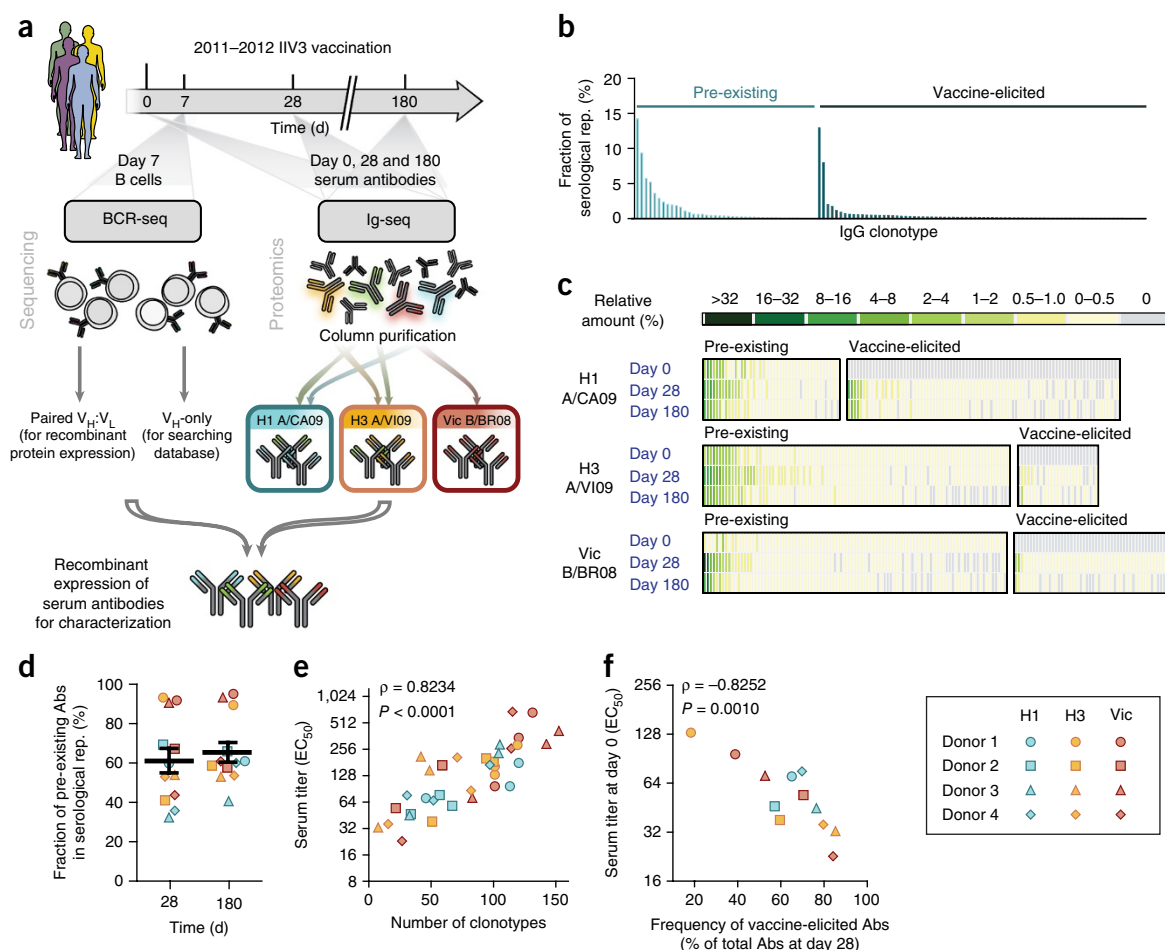


**Figure 1** Delineation of the serological repertoire to IIV3. **(a)** Experimental design. For the sequencing of B cell receptor (BCR)-encoding transcripts (BCR-seq), we used peripheral B cells isolated 7 d after vaccination to sequence the V<sub>H</sub> repertoires for constructing custom databases of each donor for heavy chain peptide identification and the paired heavy and light chain (V<sub>H</sub>:V<sub>L</sub>) repertoire for acquiring the endogenous light-chain information for the heavy chains. From sera of the donors, antibodies specific to each IIV1 were isolated through IIV1-immobilized column purification, and the purified immunoglobulins were subsequently analyzed proteomically (Ig-seq). Representative serum antibodies were recombinantly expressed for characterization. **(b)** Representative serological repertoire (rep.) (of  $n = 36$  that we analyzed) (donor 1, day 28 anti-H1 A/CA09). Each bar represents a unique clonotype, and the y axis indicates the relative abundance (fraction), as determined by proteomic analysis. **(c)** Heat maps of the relative amounts of antibody clonotypes (each column indicates distinct clonotype) comprising the serological repertoire to each IIV1 at different time points for donor 1. The amount of each clonotype is determined by multiplying its relative abundance by the serum titer for that sample. Relative amounts are determined by normalizing the amounts to day 28 serum titers (Online Methods). Similar analyses were done for all of the donors ( $n = 4$ ). **(d)** Predominance of pre-existing antibody clonotypes (Abs) in serum after vaccination. Each data point (see key) corresponds to the fraction of pre-existing Abs in the serological repertoire to an IIV1 for a specific donor. Averages are calculated as mean, with error-bars indicating s.e.m. ( $n = 12$  for each group). Vic, Victoria. **(e)** Correlation between ELISA serum titer to IIV1 and the number of clonotypes in the respective serum repertoires. Each data point corresponds to titers and the number of clonotypes in the serological repertoire specific to an IIV1 for a donor at each time point ( $n = 36$ ). **(f)** Inverse correlation between pre-vaccination ELISA serum titers and the frequency of vaccine-elicited clonotypes at day 28. Frequency is calculated as the number of vaccine-elicited clonotypes divided by the total number of unique clonotypes at day 28. For **e,f**, statistical analyses were performed using two-sided nonparametric Spearman rank correlation test.

### Prevalence of cross-reactive serum antibodies

We noticed that a unexpectedly high number of the same antibody clonotypes were detected in both the H1 A/CA09 and H3 A/VI09 affinity chromatography eluates (**Supplementary Data 1**). We considered the possibility that these antibody clonotypes may have been isolated because they bound to constituents in the vaccine other than HA, or because of nonspecific binding. However, when we proteomically analyzed the affinity chromatography eluate from donor 1 day 28 serum using recombinant HA (rHA) of A/California/07/2009 X-181, >70% (by abundance) of all of the antibody clonotypes found in the eluate from affinity chromatography with immobilized H1 A/CA09 (IIV1) were also detected in the eluate from affinity chromatography with the rHA (**Supplementary Fig. 3** and **Supplementary Data 2**).

In addition, the abundance of the H3 A/VI09-specific antibody that was also detected in the anti-H1 A/CA09 serological repertoire, on the basis of the proteomic analysis, was in excellent agreement with biochemical estimates of the abundance of H3 A/VI09-binding antibodies found in the eluate from H1 A/CA09 affinity purification (see **Supplementary Fig. 3d** for data and experimental details). These data suggest that the antibodies found in the H1 A/CA09 and in the H3 A/VI09 affinity chromatography eluates overwhelmingly recognize both of the respective HAs and are not directed to other vaccine components, such as neuraminidase.

We designated the clonotypes detected in separate affinity chromatography eluates with H1 A/CA09 and H3 A/VI09 as 'H1 + H3 cross-reactive' (**Fig. 2a** and **Supplementary Data 3**). Notably, several

highly abundant clonotypes were H1 + H3 cross-reactive, which was unexpected because previous reports on the HA specificity of antibodies isolated by single B cell cloning from IIV3 vaccine recipients had suggested that clones capable of binding to both group 1 and group 2 strains are rare<sup>13,14</sup>. In the serum samples from the four donors we analyzed, the average fractions of H1 + H3 cross-reactive antibodies among total IIV1-binding repertoire were 43.9%, 32.7% and 39.0% on days 0, 28 and 180, respectively (Fig. 2b). Also, across all donors, 63.1% of H1 + H3 cross-reactive clonotypes were pre-existing, and a higher amount of H1 + H3 cross-reactive antibodies in serum at day 0 correlated with a lower frequency of newly elicited H1 + H3 cross-reactive clonotypes at day 28 (Spearman correlation =  $-0.86$ ,  $P = 0.0107$ ; Fig. 2c), in agreement with the model in Supplementary Figure 2. Comparison of the molecular features of H1 + H3 cross-reactive antibodies with those of antibodies detected only in the anti-H1 A/CA09 or anti-H3 A/VI09 repertoires (assigned as 'H1-specific' and 'H3-specific', respectively) showed no significant differences in immunoglobulin heavy chain variable (*IGHV*) gene usage, CDR-H3 length, hydrophobicity or charge, suggesting that there are no specific B cell evolutionary trajectories or germline features that predispose antibodies toward H1 + H3 cross-reactivity (Supplementary Fig. 4).

### Functional and structural characterization of H1 + H3 cross-reactive antibodies

Because our methodology relies on the determination of the serum antibody repertoire at the CDR-H3 clonotypic level, there is a possibility that CDR-H3 peptides found in the affinity chromatography elution with both H1 A/CA09 and H3 A/VI09 might correspond to two distinct antibodies that have the same CDR-H3 but different somatic mutations, such that one antibody binds to H1 and the other to H3. To address this question, we recombinantly expressed seven H1 + H3 cross-reactive antibodies (including some of the most abundant ones) from donors 1 and 2 (Supplementary Table 5). We determined the full-length heavy and light chain ( $V_L$ ) sequences from the proteomics data and our paired  $V_H$ : $V_L$  sequence database. For two very highly abundant antibody clonotypes for which the  $V_L$  sequence was not found in the paired  $V_H$ : $V_L$  database, cognate light chains were identified by screening antigen-binding fragment (Fab)-encoding libraries constructed using the proteomically identified  $V_H$  combinatorially paired with  $V_L$ -encoding cDNA from day 7 B cells. For both  $V_H$  libraries, we isolated multiple  $V_L$  sequences with very similar CDR-L3 sequences with the same immunoglobulin kappa light chain variable (*IGKV*) and junctional (*IGKJ*) genes, suggesting that screening had converged onto a light chain that is likely to be clonally related to the respective natively paired sequences. Seven of seven H1 + H3 cross-reactive antibodies we identified proteomically bound to both IIV1s. Furthermore, five of seven H1 + H3 cross-reactive antibodies had exceptional binding breadth toward a diverse panel of rHAs from influenza groups 1 and 2, with 50% effective concentration ( $EC_{50}$ ) values  $<100$  nM, as assessed by ELISA (and apparent  $K_d$  values between 2.5 pM and 160 nM, on the basis of surface plasmon resonance analysis; Fig. 3a, Supplementary Fig. 5 and Supplementary Table 6). One additional antibody isolated from donor 1 (D1 H3-11), which was originally identified only in the H3 A/VI09 eluate, also bound to rHAs from groups 1 and 2; however, because it bound to H1 A/CA09 (IIV1) with such low affinity, it was not detected in the H1 A/CA09 eluate.

Two antibodies, D1 H1-6/H3-2 and D1 H1-9/H3-7, bound only to the H1 A/CA09 and H3 A/VI09 monovalent vaccines, but not to the respective rHAs. Consistent with this finding, these two antibodies

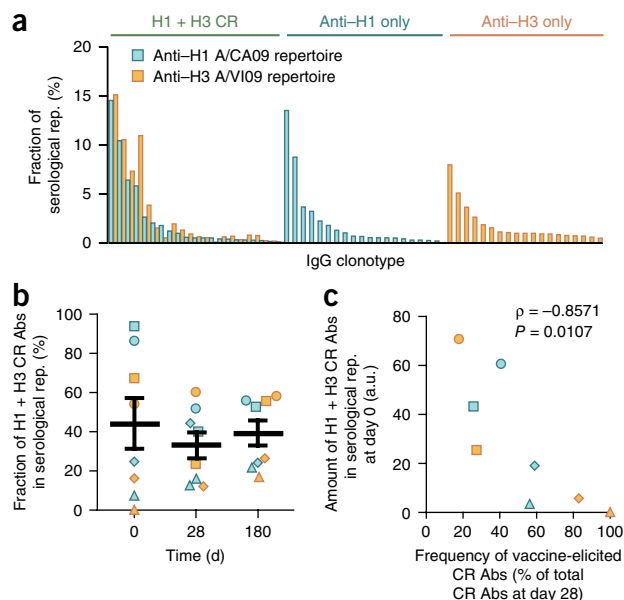


**Figure 2** Analysis of H1 + H3 cross-reactive serological repertoire. (a) Representative histogram from donor 1, day 28 anti-influenza A serological repertoire. The fraction of each antibody clonotype in the anti-H1 A/CA09 and anti-H3 A/VI09 repertoires are indicated. CR, cross-reactive. Similar analyses were done for all of the donors ( $n = 4$ ) for two antigens at three time points (total  $n = 24$  serological repertoires). (b) Relative abundance of H1 + H3 CR antibody clonotypes in the serum repertoires. Averages are calculated as the mean, with error bars indicating s.e.m. ( $n = 8$  for each group). (c) Inverse correlation between pre-vaccination amount of H1 + H3 CR antibodies and the frequency of vaccine-elicited CR antibodies at day 28. y axis indicates the amount of H1 + H3 CR antibodies in sera at day 0, and x axis indicates the frequency of vaccine-elicited CR antibodies, calculated as the number of vaccine-elicited cross-reactive clonotypes divided by the total number of cross-reactive clonotypes at day 28. Amounts were calculated as described in Figure 1c, and statistical analyses were performed using a two-sided nonparametric Spearman rank correlation test. Symbols in b,c are defined in the key for Figure 1d–f. a.u., arbitrary units.

were detected in the proteomic analysis of the affinity chromatography eluate with H1 A/CA09 but not with rHA A/California/07/2009 X-181 (Supplementary Data 2). These antibodies did not bind to neuraminidase, gelatin or other constituents of the monovalent vaccines. Notably, D1 H1-9/H3-7 neutralized group 1 and group 2 strains in pseudotyped particle-entry inhibition (PVN) assays with pandemic influenza A/California/07/2009 (H1N1) and A/Perth/16/2009 (H3N2) strains, and it bound to HA on the surface of infected Madin–Darby canine kidney (MDCK) cells (Fig. 3a,b and Supplementary Fig. 6). We concluded that D1 H1-9/H3-7 recognizes an epitope that is present in the conformation that HA assumes on the surface of infected cells but is inaccessible in purified rHA.

Although none of the eight H1 + H3 cross-reactive antibodies showed HAI activity, four of eight antibodies showed neutralization activity in PVN assays (Fig. 3a, top panel). Two of these (D1 H1-1/H3-1 and D1 H3-11) competed with the stem-binding bNAbs FI6 (ref. 10) (Supplementary Fig. 7a), and these stem-binding H1 + H3 cross-reactive antibodies were prevalent in the serum of donor 1 (D1 H1-1/H3-1 accounted for 14.2% and 14.9% of the H1 A/CA09 and H3 A/VI09 repertoires at day 28, respectively). D1 H1-1/H3-1 in particular neutralized numerous influenza virus strains in PVN assays (Supplementary Table 7). However, both antibodies had very weak or no activity in the



# ARTICLES

more physiologically relevant plaque reduction assays (**Supplementary Table 8**) and, notably, did not confer protection against infection with the H1N1 virus strain in lethal-challenge experiments in mice when administered at 5 mg per kg body weight (mg/kg) (**Fig. 3c**).

The remaining four of eight H1 + H3 cross-reactive antibodies showed no neutralization activity in HAI, PVN or plaque reduction assays (**Fig. 3a**, bottom and **Supplementary Table 8**). Three of these (D1 H1-3/H3-3, D1 H1-17/H3-14 and D2 H1-1/H3-1), which were

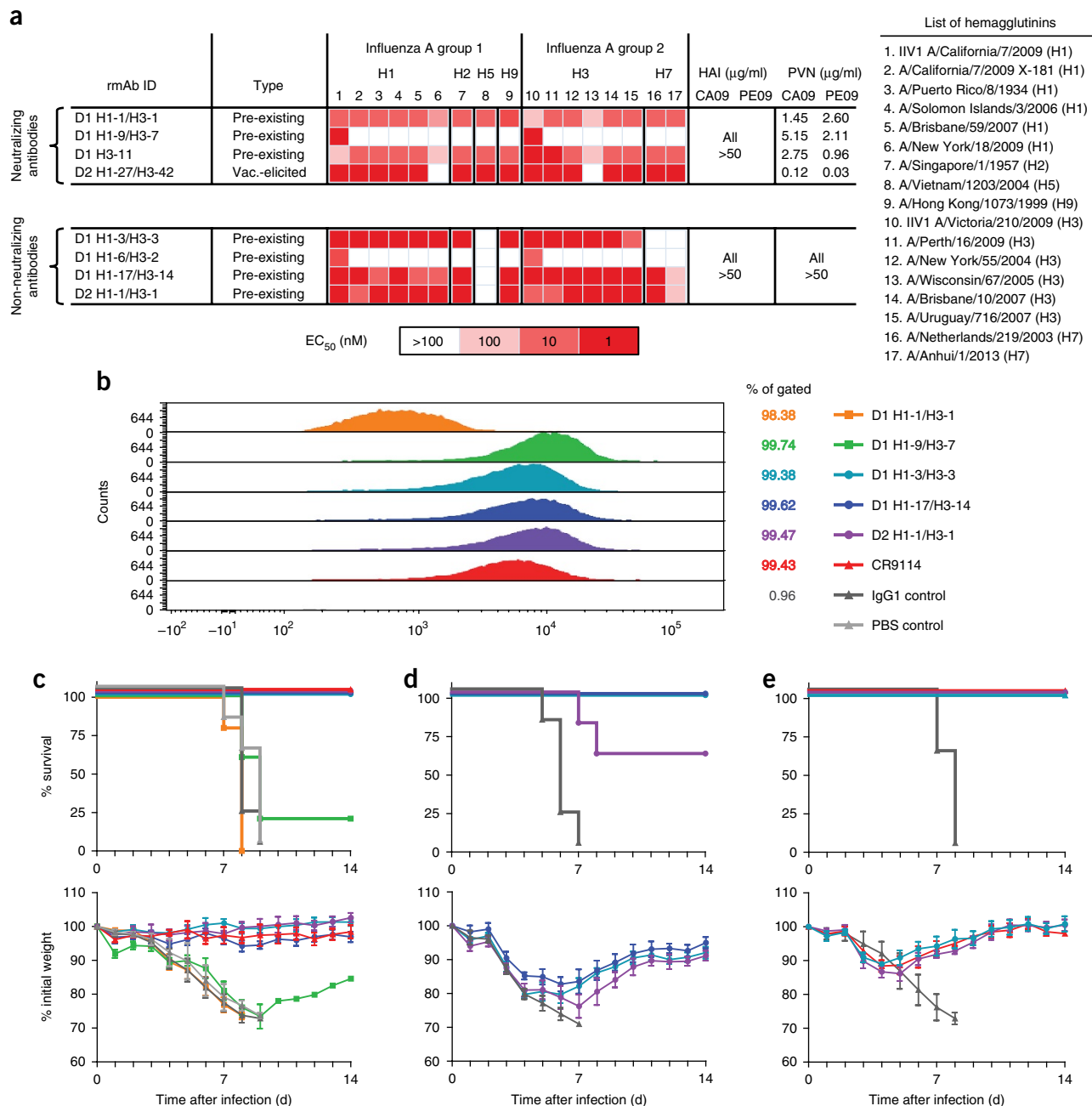


**Figure 3** Biochemical and functional analysis of the recombinantly expressed H1 + H3 CR serum antibodies. **(a)** Binding and functional characteristics. Recombinant monoclonal antibody ID (rmAb ID) indicates the donor information, as well as the abundance rankings of the antibody at day 28 in respective repertoire (i.e., D1 H1-1/H3-1 indicates that this antibody is from donor 1 and ranked first in abundance in the anti-H1 A/CA09 repertoire and first in the anti-H3 A/VI09 repertoire). EC<sub>50</sub> values, as determined by ELISA, for each recombinant antibody tested against IIV1s or rHAs as listed are shown according to the color scheme included. A/California/7/2009 (CA09) and A/Perth/16/2009 (PE09) strains were used for both the HAI and PVN assays. All assays were repeated in triplicate. **(b)** Binding of H1 + H3 CR antibodies to the HAs on the surface of the MDCKs infected with the 2009 pandemic H1N1 strain (A/Netherlands/602/09; NL09), as analyzed by FACS. 50,000 events/sample were collected using the gating scheme included in **Supplementary Figure 6**. **(c)** Survival data (Kaplan–Meier plots) (top) and weight loss data (bottom) for BALB/c mice ( $n = 5$  per group) after passive immunization (5 mg/kg) with H1 + H3 CR antibodies followed by challenge with NL09. **(d)** Survival (top) and weight loss (bottom) data for BALB/c mice ( $n = 5$  per group) after passive immunization (5 mg/kg) with the protective antibodies from **c** followed by challenge with H3N2 strain X-31 (A/Hong Kong/1/68 in the backbone of A/PR/8/34). **(e)** Survival (top) and weight loss (bottom) data for BALB/c mice ( $n = 10$  per group) challenged with NL09, followed by therapeutic administration of antibodies (5 mg/kg) at 48 h.p.i. For **c–e**, averages were calculated as mean, with error bars indicating s.d.

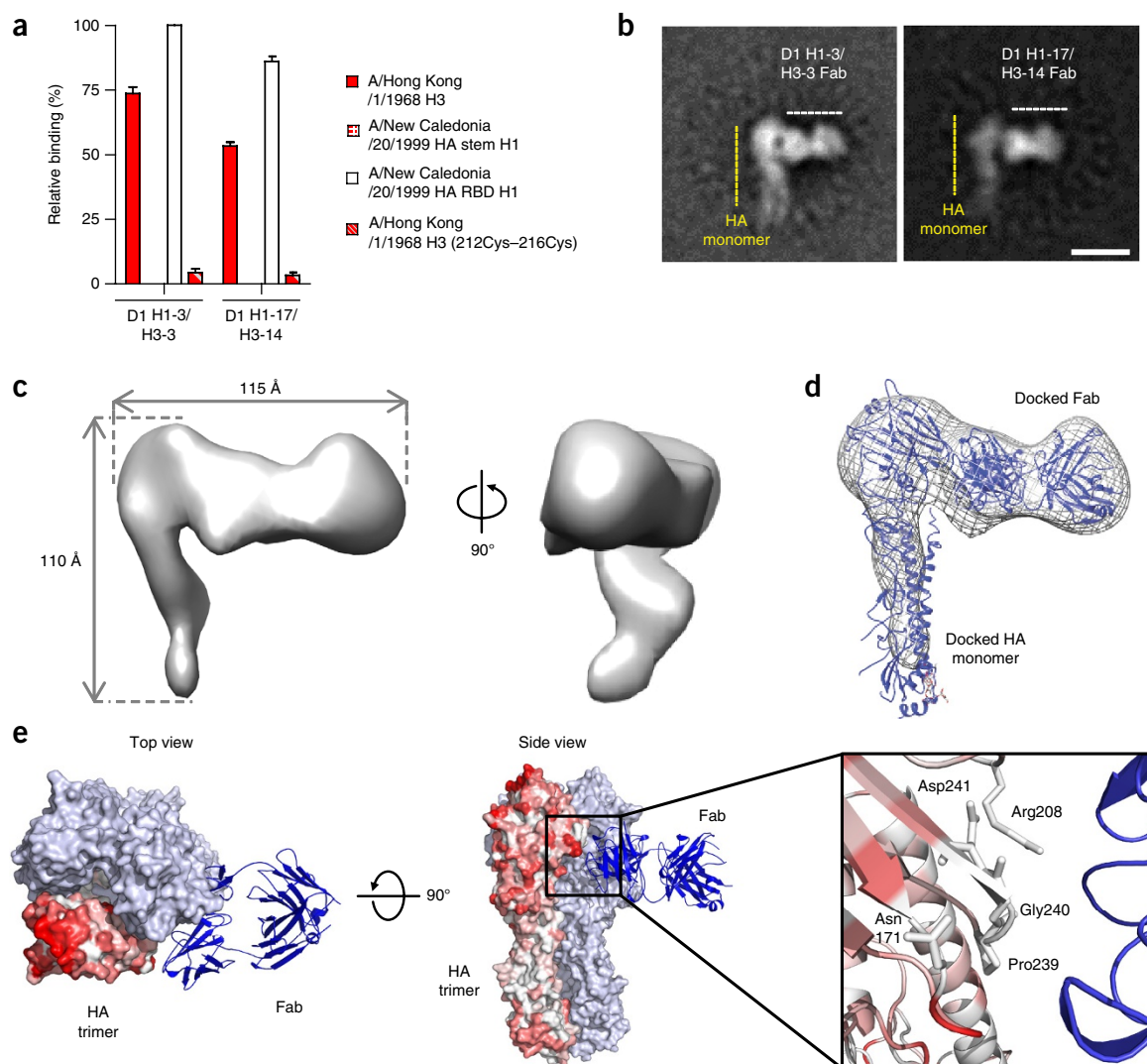


**Figure 4** Structural analysis of H1 + H3 CR antibodies. **(a)** Binding characteristics to head versus stem HA, as determined by biolayer interferometry, repeated in triplicate. H1 + H3 CR Abs bind to the RBS of the HA molecule. D1 H1-3/H3-3 and D1 H1-17/H3-14 antibodies bound with high affinity to full-length HA (A/Hong Kong/1/1968 H3) and the RBS domain (A/New Caledonia/20/1999 HA RBD H1), whereas minimal binding was observed to a stabilized stem HA (A/New Caledonia/20/1999 HA stem H1) construct or to a covalent HA trimer molecule (A/Hong Kong/1/1968 H3 (212Cys-216Cys)). **(b)** Analysis of HA-Fab complexes by negative-stain EM shows that the antibody binds to a HA monomer. Scale bar, 100 Å. **(c)** EM structure of D1 H1-3/H3-3 in complex with HA, determined to 22 Å using the random conical-tilt method. **(d)** Combined electron-density map of a single HA protomer and antibody Fab that were docked separately. **(e)** The fitted HA protomer-Fab complex was overlaid with an intact HA trimer (colored red-to-white indicating influenza HA conservation for one protomer; light blue for the remaining two protomers) showing that major overlap occurs between the Fab and an adjacent protomer molecule, which precludes binding of the antibodies to intact trimers. A set of highly conserved residues is located in this region (inset), which likely forms part of this antibody epitope.

highly abundant in both donors, competed with each other for binding to HA (**Supplementary Fig. 7b**), indicating that they target either the same or overlapping epitopes. Of note, administration of these three antibodies at 5 mg/kg, and even at lower doses (1.0 and 0.5 mg/kg), conferred excellent protection in mice that were challenged with the H1N1 strain (**Fig. 3c** and **Supplementary Fig. 8**). Furthermore, D1 H1-3/H3-3 and D1 H1-17/H3-14 also conferred 100% protection (although transient weight loss was observed) in challenge experiments with the H3N2 strain (**Fig. 3d**). Finally, treatment with D1 H1-3/H3-3 and D2 H1-1/H3-1 both led to a reduction in viral titers in the lower lung, following H1N1 challenge, and also conferred protection when administered therapeutically 24 and 48 h after infection with the H1N1 strain (**Fig. 3e** and **Supplementary Fig. 9**).

To identify the epitope targeted by the three non-neutralizing yet *in vivo*-protective antibodies (D1 H1-3/H3-3, D1 H1-17/H3-14 and D2 H1-1/H3-1), we used negative-staining electron microscopy (EM). We first tested the binding of these antibodies to multiple rHA proteins, as well as to smaller rHA domains, and although no binding was observed to a trimeric rHA stem molecule<sup>39</sup>, strong binding was observed to the rHA RBS<sup>40</sup>. The antibodies bound to the full-length rHA molecule (A/Hong Kong/1-4-MA21-1/1968) but not to a disulfide-bonded covalent trimer version of the rHA (A/Hong Kong/1-4-MA21-1/1968 212Cys-216Cys)<sup>41</sup> (**Fig. 4a**). When we mixed Fab fragments with the trimeric, full-length rHA molecules (A/Hong Kong/1-4-MA21-1/1968), we observed dissociation of the rHA trimer molecule with ~50% of the mixture, forming a 1:1 complex

## ARTICLES

of one HA protomer with one Fab molecule as shown by negative-stain EM (Fig. 4b and Supplementary Fig. 10). To visualize the epitope on the HA protomer, a three-dimensional negative-stain EM map at ~22-Å resolution was determined by using random conical tilt. A single HA protomer and an Fab molecule could be fit to the EM map (Fig. 4c,d), indicating that the antibody's mode of binding was incompatible with an intact HA trimer molecule owing to steric clashes. Competition assays with the F005-126 antibody<sup>42</sup> (Supplementary Fig. 11) and analysis of the Fab contact site on the HA molecule indicated that the antibodies (D1 H1-3/H3-3, D1 H1-17/H3-14 and D2 H1-1/H3-1) bind to a highly conserved region of the rHA molecule located on the RBS that includes Asn171, Arg208, Pro239, Gly240 and Asp241, which is occluded in the intact HA trimer (Fig. 4e). These residues are highly conserved in the HA sequence database of more than 4,468 sequences from human-infecting strains, especially for H1 and H3 strains.

### H1- or H3-specific antibody repertoire analysis

Analysis of H1- or H3-specific antibodies revealed that vaccine-elicited antibody clonotypes (as opposed to pre-existing antibodies detected at day 0) in sera were overwhelmingly either H1-specific or H3-specific (Fig. 5a). The total amount of these H1- or H3-specific antibody clonotypes correlated with the HAI titer (Spearman correlation = 0.85,  $P < 0.0001$ ; Fig. 5b and Supplementary Table 9). Because a large fraction of the serum repertoire comprises pre-existing antibodies that bind to conserved epitopes in HA (Fig. 2b), the response to the vaccine seems to become focused on new epitopes in the head domain, the region of HA that experiences the highest degree of evolutionary drift.

As expected, recombinant antibodies identified exclusively in the eluate from H1 affinity chromatography bound only to H1 A/CA09 and not to the H3 strains, and vice versa (Supplementary Fig. 12 and Supplementary Tables 5 and 6). All of the H1-specific antibodies competed for the same epitope as the RBS-targeting antibody C05 (ref. 43) (Supplementary Fig. 7c), and most of them showed activity in HAI assays, indicating that they target the RBS. One antibody, D1 H3-9, neutralized the A/Perth/16/2009 (H3N2) strain in PVN assays and also bound with high affinity to a number of recent historical group 2 rHAs (Supplementary Fig. 12).

### Anti-influenza B repertoire analysis

Influenza B is antigenically distinct from influenza A strains. Globally, quadrivalent inactivated influenza vaccines (IIV4) that include both Yamagata and Victoria lineage HAs are gradually replacing the trivalent vaccine (IIV3), which contains one B lineage strain. Whether the IIV4 offers increased protection over IIV3 is actively debated<sup>44,45</sup>. We evaluated the degree to which antibodies comprising the influenza B serum repertoires elicited by IIV3 containing a Victoria lineage strain ('Vic B/BR08' in Fig. 1) also bound to a Yamagata lineage strain, specifically the influenza B component from the 2012–2013 IIV3 (B/Texas/6/2011, abbreviated as 'Yama B/TX11'). The fraction of antibody clonotypes detected in the eluate from Vic B/BR08 enrichment and also in the eluate with immobilized Yama B/TX11, designated as 'Vic + Yama cross-reactive', comprised 95.8%, 86.6% and 83.9% of the anti-influenza B serum repertoires at days 0, 28 and 180, respectively (Fig. 5c). Five antibodies that were identified as Vic + Yama cross-reactive from donor 1, including one antibody that constituted ~40% of the anti-Vic B/BR08 repertoire, were recombinantly expressed, and their binding affinities to a panel of Victoria and Yamagata rHA proteins and their HAI titers to the vaccine strain

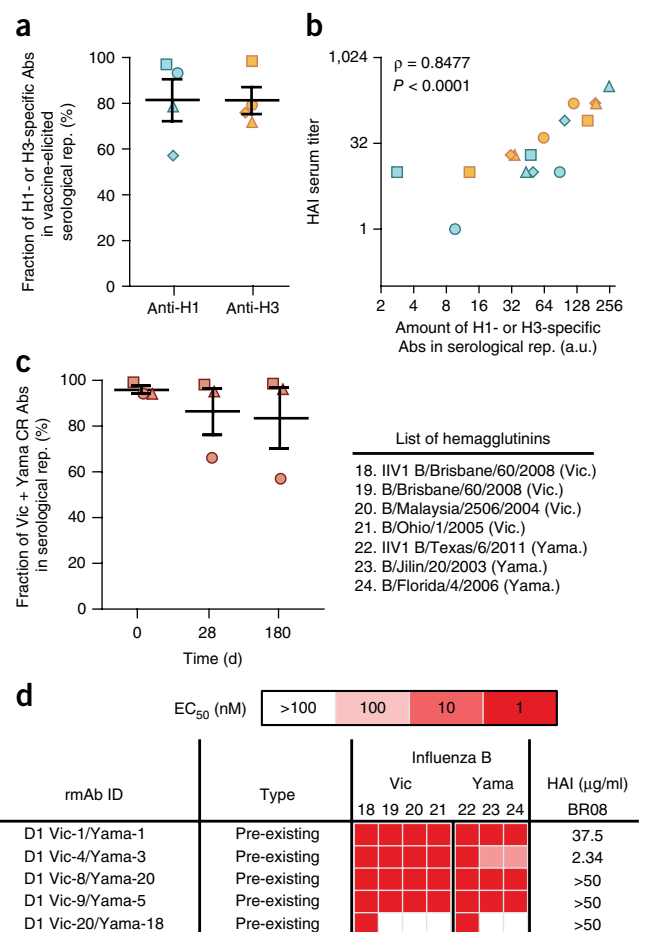


**Figure 5** Analysis of H1- or H3-specific, and influenza B-specific, serological repertoire. **(a)** Quantification of H1- or H3-specific antibodies in the vaccine-elicited antibody repertoire at day 28. Averages were calculated as mean, with error bars indicating s.e.m. ( $n = 4$  for each group). **(b)** HAI serum titers before and after vaccination as a function of the amount of H1- or H3-specific antibodies in serum before and after vaccination. Amounts were calculated as described in Figure 1c, and statistical analyses were performed using a two-sided nonparametric Spearman rank correlation test. a.u., arbitrary units. **(c)** Prevalence of Vic + Yama CR antibodies in serum. Average was calculated as the mean, with bars indicating s.e.m. ( $n = 3$  for each group). Symbols in a–c are defined in the key for Figure 1d–f. **(d)** Binding and functional characteristics of recombinantly expressed influenza B-specific serum antibodies. EC<sub>50</sub> values, as determined by ELISA, for each recombinant antibody tested against IIV1s or rHAs is listed. HAI assays were performed with B/ Brisbane/60/2008 (BR08). All assays were repeated in triplicate.

were determined (Fig. 5d and Supplementary Tables 6 and 10). Four of five antibodies bound with high affinity to all influenza B rHAs tested, whereas one antibody bound only to both Vic B/BR08 and Yama B/TX11 IIV1s but not to the respective rHAs. Our data show that most of the serum antibodies elicited by vaccination with Vic B/BR08 also bind to Yama B/TX11. This finding raises the question of whether vaccination with the new IIV4 can offer substantial additional protection benefit over that with IIV3.

### DISCUSSION

We used LC–MS/MS proteomic spectrometry of antigen-specific antibodies (Ig-seq) in combination with high-throughput sequencing of B cell transcripts (BCR-seq), to characterize, in a quantitative fashion,

the serological repertoire to each of the monovalent components of the IIV3 influenza vaccine and how the serological repertoire changes before and after immunization. Although we analyzed a relatively small cohort because of limitations imposed by the labor involved and the LC–MS/MS instrument time requirements, our data reveal a number of findings that could not have been inferred from classical serology assays (i.e., ELISA and HAI titers) or from peripheral B cell cloning or sequencing. This is because bulk serological analysis cannot provide information on the properties or the persistence of the constituent individual antibodies. Similarly, the peripheral B cell repertoire cannot be used to infer the serological antibody repertoire because: (i) the former is much more diverse than the latter; (ii) at steady-state, serological memory arises from antibodies produced by bone marrow plasma cells and not by peripheral B cells; (iii) blood samples capture a tiny fraction of the diversity of the peripheral B cell repertoire; and finally (iv) a clear negative correlation has been demonstrated between pre-existing serum antibody levels and the breadth of the B cell response, which is further correlated with age (or immune history)<sup>28</sup>, an ‘immunologic paradox’ recognized a half-century ago<sup>46</sup>.

It has been known for many years that influenza-specific antibody response after vaccination is shaped by pre-exposure history<sup>29,37,38,47</sup>. However, what could not be evaluated from bulk serological studies is the relative contribution of pre-existing circulating antibodies that are boosted by vaccination relative to that of the new, vaccine-elicited antibodies. We now show that a substantial portion (on average ~60% across all IIV1 repertoires in our cohorts as shown in **Fig. 1**) of the serum response to influenza is due to the boosting effect of pre-existing antibody clonotypes. The fraction of the serum response that arises from the boosting of pre-existing antibodies and, conversely, the clonotypic diversity of ‘new’, or vaccine-elicited, antibodies are strongly correlated with the serum titer before vaccination. In other words, high serum titer before vaccination results in a more dominant boost effect of pre-existing antibodies and the emergence of fewer vaccine-elicited antibodies, and vice versa.

The boosting of pre-existing antibodies is not necessarily detrimental for protection. For example, we showed that monomeric HA-head-specific H1 + H3 cross-reactive antibodies that conferred protection to challenge with influenza virus strains in the murine model were primarily pre-existing and were boosted significantly by vaccination (**Fig. 3**). However, given that the residues around the RBS are subject to intense evolutionary pressure, pre-existing antibodies are less likely to contribute to the increase in the HAI titer for a divergent strain. Instead, we show that the HAI titer increase after vaccination correlates with the fraction of newly elicited antibodies that is predominantly specific for one IIV1 component (**Fig. 5**), in contrast to the pre-existing, cross-reactive antibodies that bind both H1 and H3 (**Fig. 2b**).

In the analysis of the serological repertoire to the groups 1 and 2 monovalent vaccine strains in IIV3, we found an unexpectedly high prevalence of antibody clonotypes that were detected in both of the respective affinity chromatography eluates. Recombinant expression of a set of such antibodies confirmed that they do indeed bind to both group 1 and group 2 HA proteins and, furthermore, that most of these show a remarkable breadth of binding, recognizing not only historical H1 and H3 strains but also binding to H2, H5, H7 and H9. The unexpectedly large fraction of H1 + H3 cross-reactive antibodies that was detected by LC–MS/MS could not have been inferred by classical serology metrics. Similarly, a high frequency of H1 + H3 antibodies had not been noted in previous analyses of peripheral B cells. There are several possible explanations for this. Single-cell cloning typi-

cally involves the analysis of small samples of peripheral B cells, and therefore, plasmablasts or memory B cells that bind to H1 + H3 could have been missed. Additionally, the emphasis of B cell analysis studies has been on neutralization, which means that H1 + H3 cross-reactive antibodies that show little or no potency in neutralization assays could have been overlooked. An additional reason may be the kinetics of expansion of the memory B cells encoding these antibodies.

We distinguished two classes of H1 + H3 cross-reactive antibodies on the basis of their epitope specificity. One class recognized H2, H5, H7 and H9 with good to moderate affinity (in addition to H1 and H3), and these antibodies were found to compete with the stem-binding bNAb FI6. Because these antibodies are present at high levels at day 0 and bind to epitope(s) that overlap those recognized by antibodies such as FI6, their existence could be interfering with the recognition of the critical protective epitopes in the stem and the elicitation of high-potency broadly protective antibodies. The second class of H1 + H3 cross-reactive antibodies, identified in multiple donors, were all shown to bind to a highly conserved epitope on monomeric HA and to confer prophylactic and therapeutic protection against challenge by both group 1 and group 2 strains despite their complete lack of neutralization activity *in vitro*. Such antibodies have not been previously described. Given that they bind to the HA molecules on the surface of infected cells (**Fig. 3b**) but lack any detectable *in vitro* neutralization activity, the ability of these antibodies to confer protection *in vivo* is probably dependent on effector functions mediated by the crystallizable fragment (Fc) portion, namely complement activation and/or antibody-dependent cellular cytotoxicity and phagocytosis<sup>20,48</sup>. Studies to determine the precise mechanism for protection are under investigation.

Finally, a very large fraction of the serum antibody repertoire elicited by immunization with a Victoria strain reacts with the following year’s Yamagata strain. The data underscore the need for further serological and epidemiological studies to define the efficacy benefit that might be expected as the current IIV3 is being replaced with IIV4.

A key to the universal influenza vaccine will be the design of immunogens that can elicit broadly protective antibodies that bind to a variety of different strains and subtypes and also provide long-term protection. Our data on the existence of broadly protective, non-neutralizing antibodies, which are present in relatively high amounts in serum, raise interesting questions in terms of their role in the prevention of influenza infections and whether it might be desirable to design universal influenza immunogens that stimulate the production or boosting of this class of antibodies, perhaps in addition to the elicitation of neutralizing antibodies.

## METHODS

Methods, including statements of data availability and any associated accession codes and references, are available in the [online version of the paper](#).

**Accession codes.** Mass spectrometry interactive virtual environment (MassIVE): the raw proteomic data with the high-throughput sequences used as search databases are available under accession code [MSV000080184](#). Genbank: gene sequences encoding antibodies in **Supplementary Tables 5 and 10** have been deposited under accession numbers [KX882685](#) through [KX882720](#).

*Note: Any Supplementary Information and Source Data files are available in the online version of the paper.*



## ACKNOWLEDGMENTS

We are grateful to C. Das for help with monoclonal antibody expression, G. Wu, S. Schätzle and Y. Wine for preliminary experiments and advice, and S. Harrison and A. Schmidt (Harvard Medical School) for providing rHAs and critical comments on the manuscript. We are indebted to Sanofi-Pasteur for their kind gift of HIV1s and to BEI Resources for rHAs. We also thank our study volunteers and S. Mackey for clinical project management, and regulatory and data management support, and S. Swope for conducting the study visits. This work was supported by NIH grants 5U19AI057234-09 (G.G.), PO1 AI089618 (G.G.) and U19 AI109946 (F.K. and P.C.W.), NIH–NCRR CTSA award number UL1 RR025744 (C.L.D.), the Intramural Research Program of the Vaccine Research Center, NIAID, NIH (M.G.J., K.L., P.V.T., A.D., B.Z., Y.Z., L.W., W.-P.K., J.R.M. and P.D.K.), federal funds from the Frederick National Laboratory for Cancer Research, NIH, under contract HHSN261200800001E and Leidos Biomedical Research, Inc. (Y.T.), DTRA contract HDTRA1-12-C-0105 (G.G.), CPRIT grant 673 RP100890 for LC–MS/MS instrumentation at University of Texas at Austin (G.G.), the Clayton Foundation (G.G.), the Centers of Influenza Virus Research and Surveillance (CEIRS) contracts HHSN272201400008C (F.K.) and HHSN272201400005C (P.C.W.), and Welch Foundation grants F1515 (E.M. Marcotte) and F1654 (A.D.E.).

## AUTHOR CONTRIBUTIONS

J.L., D.R.B., C.V., G.C.I. and G.G. conceived and designed the research; C.L.D. was responsible for human subject aspects and conducting the clinical study; J.L., V.C., M.G.J., C.V., K.L., B.J.D., C.-H.L., J.L., E.M. Murrin, Y.T., P.V.T., A.D., B.Z., Y.Z., L.W., W.-P.K. and L.I.P. performed experiments; J.L., D.R.B., V.C., M.G.J., C.V., K.L., A.P.H., B.J.D., C.-H.L., C.C., K.H.H., Y.T., W.-P.K., D.P., L.I.P., M.M.D., C.E.C., T.M.R., A.D.E., P.C.W., E.M. Marcotte, J.R.M., G.C.I., F.K., S.R.Q., P.D.K. and G.G. analyzed data; and J.L., D.R.B., M.G.J., G.C.I., P.D.K. and G.G. wrote the paper.

## COMPETING FINANCIAL INTERESTS

The authors declare no competing financial interests.

Reprints and permissions information is available online at <http://www.nature.com/reprints/index.html>.

- Molinari, N.-A.M. *et al.* The annual impact of seasonal influenza in the US: measuring disease burden and costs. *Vaccine* **25**, 5086–5096 (2007).
- Lambert, L.C. & Fauci, A.S. Influenza vaccines for the future. *N. Engl. J. Med.* **363**, 2036–2044 (2010).
- Rimmelzwaan, G.F. & McElhaney, J.E. Correlates of protection: novel generations of influenza vaccines. *Vaccine* **26**, D41–D44 (2008).
- Krammer, F. & Palese, P. Advances in the development of influenza virus vaccines. *Nat. Rev. Drug Discov.* **14**, 167–182 (2015).
- Monto, A.S. *et al.* Comparative efficacy of inactivated and live attenuated influenza vaccines. *N. Engl. J. Med.* **361**, 1260–1267 (2009).
- Osterholm, M.T., Kelley, N.S., Sommer, A. & Belongia, E.A. Efficacy and effectiveness of influenza vaccines: a systematic review and meta-analysis. *Lancet Infect. Dis.* **12**, 36–44 (2012).
- Hobson, D., Curry, R.L., Beare, A.S. & Ward-Gardner, A. The role of serum haemagglutination-inhibiting antibody in protection against challenge infection with influenza A2 and B viruses. *J. Hyg. (Lond.)* **70**, 767–777 (1972).
- Hannoun, C., Megas, F. & Piercy, J. Immunogenicity and protective efficacy of influenza vaccination. *Virus Res.* **103**, 133–138 (2004).
- Okuno, Y., Isegawa, Y., Sasao, F. & Ueda, S. A common neutralizing epitope conserved between the hemagglutinins of influenza A virus H1 and H2 strains. *J. Virol.* **67**, 2552–2558 (1993).
- Corti, D. *et al.* A neutralizing antibody selected from plasma cells that binds to group 1 and group 2 influenza A hemagglutinins. *Science* **333**, 850–856 (2011).
- Dreyfus, C. *et al.* Highly conserved protective epitopes on influenza B viruses. *Science* **337**, 1343–1348 (2012).
- Li, G.-M. *et al.* Pandemic H1N1 influenza vaccine induces a recall response in humans that favors broadly cross-reactive memory B cells. *Proc. Natl. Acad. Sci. USA* **109**, 9047–9052 (2012).
- Wrammert, J. *et al.* Rapid cloning of high-affinity human monoclonal antibodies against influenza virus. *Nature* **453**, 667–671 (2008).
- Moody, M.A. *et al.* H3N2 influenza infection elicits more cross-reactive and less clonally expanded anti-hemagglutinin antibodies than influenza vaccination. *PLoS One* **6**, e25797 (2011).
- Nakamura, G. *et al.* An *in vivo* human-plasmablast-enrichment technique allows rapid identification of therapeutic influenza A antibodies. *Cell Host Microbe* **14**, 93–103 (2013).
- Wrammert, J. *et al.* Broadly cross-reactive antibodies dominate the human B cell response against 2009 pandemic H1N1 influenza virus infection. *J. Exp. Med.* **208**, 181–193 (2011).
- Ellebedy, A.H. *et al.* Induction of broadly cross-reactive antibody responses to the influenza HA stem region following H5N1 vaccination in humans. *Proc. Natl. Acad. Sci. USA* **111**, 13133–13138 (2014).
- Whittle, J.R.R. *et al.* Flow cytometry reveals that H5N1 vaccination elicits cross-reactive stem-directed antibodies from multiple Ig heavy-chain lineages. *J. Virol.* **88**, 4047–4057 (2014).
- Baz, M. *et al.* Seroconversion to seasonal influenza viruses after A(H1N1)pdm09 virus infection, Quebec, Canada. *Emerging Infect. Dis.* **18**, 1132–1134 (2012).
- DiLillo, D.J., Palese, P., Wilson, P.C. & Ravetch, J.V. Broadly neutralizing anti-influenza antibodies require Fc receptor engagement for *in vivo* protection. *J. Clin. Invest.* **126**, 605–610 (2016).
- Henry Dunand, C.J. *et al.* Both neutralizing and non-neutralizing human H7N9 influenza vaccine-induced monoclonal antibodies confer protection. *Cell Host Microbe* **19**, 800–813 (2016).
- Radigan, K.A., Misharin, A.V., Chi, M. & Budinger, G.S. Modeling human influenza infection in the laboratory. *Infect. Drug Resist.* **8**, 311–320 (2015).
- Wohlbolt, T.J. *et al.* Hemagglutinin stalk- and neuraminidase-specific monoclonal antibodies protect against lethal H10N8 influenza virus infection in mice. *J. Virol.* **90**, 851–861 (2015).
- Whittle, J.R.R. *et al.* Broadly neutralizing human antibody that recognizes the receptor-binding pocket of influenza virus hemagglutinin. *Proc. Natl. Acad. Sci. USA* **108**, 14216–14221 (2011).
- Lee, P.S. *et al.* Receptor mimicry by antibody F045-092 facilitates universal binding to the H3 subtype of influenza virus. *Nat. Commun.* **5**, 3614 (2014).
- Krause, J.C. *et al.* A broadly neutralizing human monoclonal antibody that recognizes a conserved, novel epitope on the globular head of the influenza H1N1 virus hemagglutinin. *J. Virol.* **85**, 10905–10908 (2011).
- Jackson, K.J.L. *et al.* Human responses to influenza vaccination show seroconversion signatures and convergent antibody rearrangements. *Cell Host Microbe* **16**, 105–114 (2014).
- Fonville, J.M. *et al.* Antibody landscapes after influenza virus infection or vaccination. *Science* **346**, 996–1000 (2014).
- Brodin, P. *et al.* Variation in the human immune system is largely driven by nonheritable influences. *Cell* **160**, 37–47 (2015).
- Andrews, S.F. *et al.* Immune history profoundly affects broadly protective B cell responses to influenza. *Sci. Transl. Med.* **7**, 316ra192 (2015).
- Vollmers, C., Sit, R.V., Weinstein, J.A., Dekker, C.L. & Quake, S.R. Genetic measurement of memory B cell recall using antibody repertoire sequencing. *Proc. Natl. Acad. Sci. USA* **110**, 13463–13468 (2013).
- Lavinder, J.J. *et al.* Identification and characterization of the constituent human serum antibodies elicited by vaccination. *Proc. Natl. Acad. Sci. USA* **111**, 2259–2264 (2014).
- Georgiou, G. *et al.* The promise and challenge of high-throughput sequencing of the antibody repertoire. *Nat. Biotechnol.* **32**, 158–168 (2014).
- DeKosky, B.J. *et al.* In-depth determination and analysis of the human paired heavy- and light-chain antibody repertoire. *Nat. Med.* **21**, 86–91 (2015).
- Boutz, D.R. *et al.* Proteomic identification of monoclonal antibodies from serum. *Anal. Chem.* **86**, 4758–4766 (2014).
- Wine, Y., Horton, A.P., Ippolito, G.C. & Georgiou, G. Serology in the 21st century: the molecular-level analysis of the serum antibody repertoire. *Curr. Opin. Immunol.* **35**, 89–97 (2015).
- Sasaki, S. *et al.* Influence of prior influenza vaccination on antibody and B cell responses. *PLoS One* **3**, e2975 (2008).
- Andrews, S.F. *et al.* High pre-existing serological antibody levels correlate with diversification of the influenza vaccine response. *J. Virol.* **89**, 3308–3317 (2015).
- Yassine, H.M. *et al.* Hemagglutinin–stem nanoparticles generate heterosubtypic influenza protection. *Nat. Med.* **21**, 1065–1070 (2015).
- Schmidt, A.G. *et al.* Viral receptor-binding site antibodies with diverse germline origins. *Cell* **161**, 1026–1034 (2015).
- Godley, L. *et al.* Introduction of intersubunit disulfide bonds in the membrane-distal region of the influenza hemagglutinin abolishes membrane fusion activity. *Cell* **68**, 635–645 (1992).
- Iba, Y. *et al.* Conserved neutralizing epitope at globular head of hemagglutinin in H3N2 influenza viruses. *J. Virol.* **88**, 7130–7144 (2014).
- Ekiert, D.C. *et al.* Cross-neutralization of influenza A viruses mediated by a single antibody loop. *Nature* **489**, 526–532 (2012).
- Jain, V.K. *et al.* Vaccine for prevention of mild and moderate-to-severe influenza in children. *N. Engl. J. Med.* **369**, 2481–2491 (2013).
- Tinoco, J.C. *et al.* Immunogenicity, reactogenicity and safety of inactivated quadrivalent influenza vaccine candidate versus inactivated trivalent influenza vaccine in healthy adults aged ≥18 years: a phase 3, randomized trial. *Vaccine* **32**, 1480–1487 (2014).
- Morris, J.A., Kasel, J.A., Saglam, M., Knight, V. & Loda, F.A. Immunity to influenza to antibody levels. *N. Engl. J. Med.* **274**, 527–535 (1966).
- Francis, T.J. On the doctrine of original antigenic sin. *Proc. Am. Phil. Soc.* **104**, 572–578 (1960).
- DiLillo, D.J., Tan, G.S., Palese, P. & Ravetch, J.V. Broadly neutralizing hemagglutinin stalk-specific antibodies require Fc-γR interactions for protection against influenza virus *in vivo*. *Nat. Med.* **20**, 143–151 (2014).

## ONLINE METHODS

**Study volunteers, peripheral blood mononuclear cell (PBMC) isolation and RNA extraction.** All study protocols were approved by the Institutional Review Boards at Stanford University. Informed consent was obtained from the participants. Blood was taken before (day 0) and after (days 7, 28 and 180) vaccination. Volunteers were four young adults (ages 22–32 years) in generally good health who were vaccinated with one dose of IIV3 (FluZone; Sanofi-Pasteur); 60 ml peripheral blood was taken from the individuals, to which heparin was added. PBMCs were extracted from 10 ml blood using a Ficoll gradient and frozen in 10% (vol/vol) DMSO/40% (vol/vol) FBS according to the protocols of the Stanford Human Immune Monitoring Center (HIMC). After thawing, total RNA was extracted from 5 million PBMCs using the Qiagen AllPrep Kit.

**Library preparation for high-throughput sequencing of  $V_H$ -encoding genes.** 500 ng of total RNA was used as input for library preparation. Reverse-transcription was performed according to the manufacturer's instructions using SuperScript III Enzyme (Life Technologies) and primers for all five isotypes containing eight random nucleotides and partial Illumina adapters containing Illumina barcodes. Second-strand synthesis was done using Phusion Polymerase (NEB), and primers containing eight random nucleotides and partial Illumina adaptor sequences that bind either framework region (FR) 1 or 3 of all variable (V) segments with a maximum of one mismatch (98 °C for 2 min, 52 °C for 2 min, and 72 °C for 10 min). Double-stranded cDNA was purified two times using Ampure XP beads at a ratio of 1:1. Double-stranded cDNA was amplified with Platinum HiFi Polymerase (Life Technologies) with two primers completing Illumina adaptor sequences (amplification conditions: 95 °C for 2 min; 27 cycles of 95 °C for 30 s, 65 °C for 30 s and 68 °C for 2 min; and 68 °C for 7 min). Final sequencing libraries were generated by purifying the PCR product using Ampure XP beads at a ratio of 1:1, and they were sequenced using the Illumina MiSeq platform.

**$V_H$ - $V_L$ -paired sequencing.** Paired heavy and light chain sequencing of single B cells from donor 1 day 7 and donor 2 day 7 samples was carried out as previously described<sup>34,49</sup>. Briefly, B cells were isolated as single cells inside emulsion droplets using a custom flow-focusing apparatus. Droplets contained lysis buffer and poly(dT)-conjugated magnetic beads, as well as lysis buffer to capture mRNAs generated by genes encoding heavy and light chain molecules. Magnetic beads were collected and emulsified to serve as template for emulsion overlap extension RT-PCR. A follow-up nested PCR generated 850-bp linked  $V_H$ - $V_L$  amplicons that were sequenced using the Illumina MiSeq platform.  $V_H$  and  $V_L$  regions were amplified separately for full-length  $V_H$  and  $V_L$  analysis for the recombinant expression of monoclonal antibodies using the Illumina MiSeq platform as previously described<sup>32,49</sup>.

**Reagents.** Individual IIV1s comprising the 2011–2012 FluZone IIV3 (H1N1 A/California/07/2009 X-179A, H3N2 A/Victoria/210/2009 X-187 and B/Brisbane/60/2008), as well as the influenza B component of the 2012–2013 FluZone IIV3 (B/Texas/6/2011), were obtained from Sanofi-Pasteur. The following reagents were obtained through BEI Resources, NIAID, NIH: H1 hemagglutinin (HA) protein from influenza virus A/Puerto Rico/8/1934 (H1N1) with a C-terminal histidine tag, recombinant from baculovirus, NR-19240; H1 HA from influenza virus A/Brisbane/59/2007 (H1N1), recombinant from baculovirus, NR-15267; H1 HA from influenza virus A/New York/18/2009 with a C-terminal histidine tag, recombinant from baculovirus, NR-19441; H2 HA from influenza virus A/Singapore/1/1957 (H2N2), recombinant from baculovirus, NR-2668; H5 HA from influenza virus A/Vietnam/1203/2004 (H5N1), recombinant from baculovirus, NR-10510; H9 HA from influenza virus A/Hong Kong/1073/1999 (H9N2), recombinant from baculovirus, NR-654; H3 HA from influenza virus A/Perth/16/2009 (H3N2) with a C-terminal histidine tag, recombinant from baculovirus, NR-42974; H3 HA from influenza virus A/New York/55/2004 (H3N2), recombinant from baculovirus, NR-19241; H3 HA from influenza virus A/Wisconsin/67/2005 (H3N2), recombinant from baculovirus, NR-15171; H3 HA from influenza virus A/Brisbane/10/2007 (H3N2), recombinant from baculovirus, NR-19238; H3 HA from influenza virus A/Uruguay/716/2007 (H3N2), recombinant from baculovirus, NR-15168;

H7 HA from influenza virus A/Netherlands/219/2003 (H7N7), recombinant from baculovirus, NR-2633; H7 HA from influenza virus A/Anhui/1/2013 (H7N9), recombinant from baculovirus, NR-45118; HA from influenza virus B/Brisbane/60/2008, recombinant from baculovirus, NR-19239; HA from influenza virus B/Malaysia/2506/2004, recombinant from baculovirus, NR-15172; HA from influenza virus B/Ohio/1/2005, recombinant from baculovirus, NR-19243; HA from influenza virus B/Jilin/20/2003, recombinant from baculovirus, NR-19242; HA from influenza virus B/Florida/4/2006, recombinant from baculovirus, NR-15169; N1 neuraminidase (NA) protein from influenza virus A/California/04/2009 (H1N1)pdm09 with an N-terminal histidine tag, recombinant from baculovirus, NR-19234. A/California/7/2009-X181 and A/Solomon Islands/3/2006 rHAs were provided by Dr. Stephen Harrison (Harvard Medical School).

**Purification of total IgG from serum and subsequent digestion into F(ab')<sub>2</sub>.** For each serum sample analyzed in this study, 30 ml of diluted serum (1:2 dilution in PBS) was passed through a 4-ml Protein G Plus agarose (Pierce) affinity column in gravity mode. Serum flowthrough was collected and passed through the column three times. The column was washed with 15 column volumes (cv) of PBS before elution with 5 cv of 100 mM glycine-HCl, pH 2.7. The eluate, containing total IgG from serum, was immediately neutralized with 2 ml of 1 M Tris-HCl, pH 8.0, and dialyzed into 20 mM sodium acetate, pH 4.5, overnight at 4 °C. Purified IgG was digested into F(ab')<sub>2</sub> with 1 ml of immobilized pepsin resin (Pierce) per 40 mg of IgG in 20 mM sodium acetate, pH 4.5, for 4 h on an inverter at 37 °C. Pepsin resin was spun down at 2,000g to halt digestion and washed with PBS three times. Supernatants from the digestion reactions and washes were combined and pH-adjusted to 7.

**Antigen-enrichment of F(ab')<sub>2</sub> and mass spectrometry sample preparation.** The respective IIV1s or rHA were immobilized on *N*-hydroxysuccinimide (NHS)-activated agarose resins (Pierce) by overnight rotation at 4 °C. The coupled agarose resins were washed with PBS, and unreacted NHS groups were blocked with 1 M ethanolamine, pH 8.3, for 30 min at room temperature (RT). The beads were further washed with PBS and packed into a 2-ml chromatography column (Clontech). The column was prewashed with 5 cv of 2 M urea and equilibrated with 10 cv of PBS. The prewashing step with urea was to remove HA that was noncovalently bound to the resin following immobilization, because we initially noticed that a large amount of HAs detaching from the resins interfered with the subsequent analysis. Exhaustive controls with elution and flow-through samples from affinity chromatography were performed to ensure that the prewashing step with 2 M urea does not impede complete capture of F(ab')<sub>2</sub> molecules that recognize IIV1.

For each sample, the F(ab')<sub>2</sub> sample was divided into equal volumes, with each fraction being applied to the individual antigen affinity columns in gravity mode. Flowthrough was collected and reapplied to the column three times, and the column was washed with 10 cv of PBS and 10 cv of diluted PBS (1:2 in ddH<sub>2</sub>O). Antigen-enriched F(ab')<sub>2</sub> was eluted with 60 mM HCl, pH 1.7, in 0.5-ml fractions and neutralized with NaOH/Tris. Flowthrough and elution fractions were assayed by indirect ELISA with the corresponding IIV1. To ensure that our enrichment steps were not biasing isolation for high-affinity antibodies, the depletion of ELISA signal in each flowthrough sample was checked. Elution fractions showing an ELISA signal were pooled and concentrated under vacuum to a volume of ~0.1 ml and desalted into ddH<sub>2</sub>O using a 0.5-ml Zeba spin column (Pierce). The desalted eluate was further concentrated to 50 µl under vacuum.

For each enrichment, elution and flowthrough samples were denatured in 50% (vol/vol) 2,2,2-trifluoroethanol (TFE), 50 mM ammonium bicarbonate and 10 mM dithiothreitol (DTT) at 60 °C for 1 h, then alkylated by incubation with 32 mM iodoacetamide (Sigma) for 1 h at RT in the dark. Alkylation was quenched by the addition of 20 mM DTT. Samples were diluted tenfold with 50 mM ammonium bicarbonate and digested with trypsin (1:30 trypsin:protein) for 16 h at 37 °C. Formic acid was added to 1% (vol/vol) to quench the digestion, and the sample volume was reduced to ~100 µl under vacuum. Peptides were then bound to a C18 Hypersep SpinTip (Thermo Scientific), washed three times with 0.1% formic acid and eluted with 60% acetonitrile, 0.1% formic acid. C18 eluate was dried under vacuum-centrifugation and resuspended in 50 µl in 5% acetonitrile, 0.1% formic acid.

**LC-MS/MS analysis.** Samples were analyzed by liquid chromatography–tandem mass spectrometry on a Dionex Ultimate 3000 RSLCnano uHPLC system (Thermo Scientific) coupled to an LTQ Orbitrap Velos Pro mass spectrometer (Thermo Scientific). Peptides were first loaded onto an Acclaim PepMap RSLC NanoTrap column (Dionex; Thermo Scientific) before separation on a 75- $\mu\text{m} \times 15\text{-cm}$  Acclaim PepMap RSLC C18 column (Dionex; Thermo Scientific) using a 5–40% (vol/vol) acetonitrile gradient over 250 min at 300 nl/min. Eluting peptides were injected directly into the mass spectrometer using a nano-electrospray source. The LTQ Orbitrap Velos Pro was operated in data-dependent mode with parent ion scans (MS1) collected at 60,000 resolutions. Mono-isotopic precursor selection and charge-state screening were enabled. Ions with a charge  $\geq +2$  were selected for collision-induced dissociation fragmentation spectrum acquisition (MS2) in the ion trap, with a maximum of 20 MS2 scans per MS1. Dynamic exclusion was active with a 45-s exclusion time for ions selected more than twice in a 30-s window. Each sample was run three times to generate technical replicate data sets.

**MS/MS data analysis.** Donor-specific protein sequence databases were constructed using the donor's  $V_H$  sequences with  $\geq 2$  reads, concatenated to a database of background proteins comprising non-donor-derived  $V_L$  sequences (HD1)<sup>32</sup>, a consensus human protein database (Ensembl 73, longest sequence per gene) and a list of common protein contaminants (MaxQuant). Donor-specific spectra were searched against the corresponding donor-specific database using SEQUEST (Proteome Discoverer 1.4; Thermo Scientific). Searches considered fully tryptic peptides only, allowing up to two missed cleavages. A precursor mass tolerance of 5 p.p.m. and a fragment-mass tolerance of 0.5 Da were used. Modifications of carbamidomethyl cysteine (static) and oxidized methionine (dynamic) were selected. High-confidence peptide-spectrum matches (PSMs) were filtered at a false discovery rate of  $< 1\%$  as calculated by Percolator ( $q$ -value  $< 0.01$ , Proteome Discoverer 1.4; Thermo Scientific).

Isoleucine/leucine sequence variants were collapsed into single peptide groups. For each scan, PSMs were ranked first by posterior error probability (PEP), then  $q$ -value, and finally XCorr. Only unambiguous top-ranked PSMs were kept; scans with multiple top-ranked PSMs (equivalent PEP,  $q$ -value and XCorr) were designated ambiguous identifications and removed. Observed precursor masses were recalibrated according to the previous method<sup>50</sup>, and the average mass deviation (AMD) for each peptide was calculated as described<sup>35</sup> using data from elutions only. Peptides with an AMD  $> 1.5$  p.p.m. were removed. Additionally, only peptides identified in  $\geq 2$  replicate injections for at least one elution sample were kept as high-confidence identifications.

Peptide abundance was calculated from the extracted-ion chromatogram (XIC) peak area, as described<sup>32</sup>, using peak area values generated by the Precursor Ions Area Detector node in Proteome Discoverer. For each peptide, a total XIC area was calculated as the sum of all unique XIC areas of associated precursor ions, and the average XIC area across replicate injections was calculated for each sample. For each antigen data set, the eluate and flowthrough abundances were compared and peptides with  $\geq 10$ -fold higher signal in the elution sample were considered to be antigen specific. Similarly, peptide abundances in elution samples were compared across antigens; peptides with  $\geq 10$ -fold higher signal for a single antigen were considered specific (i.e., H1 or H3 specific), and peptides with  $< 10$ -fold difference for two or more antigens were considered cross-reactive (i.e., H1 + H3 cross-reactive). In addition, in our H1 + H3 cross-reactive serological repertoire analysis, to avoid overestimating, we removed peptides that appeared in the eluates of all three IIV1 enrichments (which could potentially be binding to other constituents in the vaccine); on average, they accounted for  $< 10\%$  (by abundance) of the serological repertoire. The resulting data sets are tabulated in **Supplementary Data 3**.

**Clonotype indexing and peptide-to-clonotype mapping.**  $V_H$ -encoding sequences were grouped into clonotypes on the basis of single-linkage hierarchical clustering as described<sup>32</sup>. Cluster membership required  $\geq 90\%$  identity across the CDR-H3 amino sequence as measured by edit distance. High-confidence peptides identified by MS/MS analysis were mapped to clonotype clusters, and peptides uniquely mapping to a single clonotype were considered 'informative'. The abundance of each antibody clonotype was calculated by summing the XIC areas of the informative peptides mapping to  $\geq 4$  amino acids of the CDR-H3 region.

**Quantitating abundances of individual antibody clonotypes.** For each serological repertoire, the relative abundance of a clonotype was calculated by dividing the XIC area for a particular clonotype by the sum of the XIC areas for all clonotypes. Fraction of serological repertoire refers to this relative abundance based on XIC. The amount for a particular clonotype was determined by multiplying its fraction of serological repertoire by the corresponding serum sample's binding titer. To generate heat maps, we accounted for the different total binding titers toward each IIV1 by normalizing amount using the day 28 titer as a reference, calling this 'relative amount'. For example, the amount for each clonotype divided by the serum titer of the day 28 sample refers to relative amount.

**Recombinant antibody synthesis, expression and purification.** Selection of antibody sequences for recombinant expression was based on the combination of  $V_H$ : $V_L$ -paired databases and proteomics data. First, we identified antibody clonotypes identified in the proteomics analysis and searched for the same clonotype in the  $V_H$ : $V_L$ -paired database. Full-length heavy- and light-chain-encoding sequences were then determined from the paired sequencing database.

For two of the recombinantly expressed antibodies (D1 H1-1/H3-1 and D1 H1-6/H3-2), their sequences were not found in the  $V_H$ : $V_L$  paired database; thus their corresponding light chains were screened in phage as previously described<sup>32</sup>. Briefly,  $\kappa$  and  $\lambda$  light chain libraries were constructed for each heavy chain by amplifying  $V_L$  sequences from cDNA of day 7 PBMCs. Individual clones from the libraries were screened on Costar 96-well ELISA plates (Corning) coated with IIV1s, and wells with signals were sequenced to identify the light chain sequences. From each screening, multiple light chains were identified; they shared the same *IGKV* and *IGKJ* genes, and had homologous CDR-L3 sequences, indicating that they are likely similar to the endogenously paired  $V_L$ .

These genes were purchased as gBlocks (Integrated DNA Technologies) and cloned into the pcDNA3.4 vector (Invitrogen). Heavy- and light-chain-encoding plasmids for each monoclonal antibody were transfected into Expi293 cells (Invitrogen) at a 1:3 ratio. After incubating for 5 d at 37 °C with 8%  $\text{CO}_2$ , the supernatant containing the secreted antibodies was collected by centrifugation at 500g for 15 min at RT. The supernatant was passed over a column with 0.5 ml Protein A agarose resin (Thermo Scientific) three times to ensure efficient capture. After washing the column with 20 cv of PBS, antibodies were eluted with 3 ml 100 mM glycine-HCl, pH 2.7, and immediately neutralized with 1 ml 1 M Tris-HCl, pH 8.0. Antibodies were buffer-exchanged into PBS using Amicon Ultra-30 centrifugal spin columns (Millipore).

**Enzyme-linked immunosorbent assays (ELISAs).**  $\text{EC}_{50}$  values based on ELISA were used to determine the binding titers of IIV1-specific antibodies in the serum samples or apparent affinities of the recombinant monoclonal antibodies. First, costar 96-well ELISA plates (Corning) were coated overnight at 4 °C with 4  $\mu\text{g/ml}$  IIV1 or recombinant HAs, and washed and blocked with 2% milk in PBS for 2 h at RT. After blocking, serially diluted recombinant antibodies or serum samples were bound to the plates for 1 h, followed by incubation with 1:5,000-diluted goat anti-human-IgG Fc horseradish peroxidase (HRP)-conjugated secondary antibodies (Jackson ImmunoResearch; 109-035-008) for 1 h. For detection, 50  $\mu\text{l}$  TMB-ultra substrate (Thermo Scientific) was added before quenching with 50  $\mu\text{l}$  1 M  $\text{H}_2\text{SO}_4$ . Absorbance was measured at 450 nm using a Tecan M200 plate reader. Data were analyzed and fitted for  $\text{EC}_{50}$  using a four-parameter logistic nonlinear regression model in the GraphPad Prism software. All ELISA assays were performed in triplicate.

**Surface plasmon resonance (SPR).** To determine the affinities of the influenza-specific recombinant antibodies toward the rHAs, a Biacore 3000 instrument (GE Healthcare) was used. Bovine serum albumin (BSA) was immobilized in the reference channels of the CM5 sensor chip to subtract the buffer effect and nonspecific binding signal, and the rHAs were immobilized in separate channels by amine-coupling at pH 5.5. All SPR measurements were performed in HBS-EP running buffer (10 mM HEPES, pH 7.4, 0.15 M NaCl, 3 mM EDTA, 0.005% vol/vol surfactant P20; GE Healthcare). The serially diluted antibodies (400–12.5 nM) were injected in triplicates at 30  $\mu\text{l/min}$  for 2 min and allowed a dissociation time of 10 min. The chip was regenerated after each binding event with 10 mM NaOH or 50 mM Tris, pH 11, with a contact time of 1 min.



The resulting sensorgrams were fit with a bivalent model using Biaevaluation 3.0 software, and the kinetic parameters were reported as the average of the three technical replicates.

To compare the binding epitopes of monoclonal antibodies, the antibodies in sodium acetate, pH 5.0 were immobilized on the CM5 sensor chips surface to a surface density of ~1,000 response units (RUs) by amine coupling. rHA at 100 µg/ml in HBS-EP were flowed over the immobilized-antibody surface at a flow rate of 30 µl/min for 2 min and, without the dissociation phase, each monoclonal antibody (at 100 µg/ml in HBS-EP) tested was immediately injected over the surface at 30 µl/min for 2 min. Between cycles, the flow cells were regenerated with 10 mM NaOH with a contact time of 1 min.

**Binding studies using biolayer interferometry.** A fortéBio Octet Red384 instrument was used to measure binding of H1 + H3 CR antibodies (D1 H1-3/H3-3 and D1 H1-17/H3-14) to influenza HA (full-length, RBD domain constructs, stem-only constructs). All of the assays were performed with agitation set to 1,000 r.p.m. in PBS buffer supplemented with 1% BSA to minimize non-specific interactions. The final volume for all the solutions was 100 µl/well. Assays were performed at 30 °C in solid black 96-well plates (Geiger Bio-One). HA molecules (35 µg/ml) in PBS buffer was used to load anti-penta His probes for 300 s. Typical capture levels were ~1 nm, and variability within a row of eight tips did not exceed 0.1 nm. Antibody binding was allowed to proceed for 300 s and normalized to a control antibody (5J8 for RBD, 39.29 for HA stem and full-length HA). Measurements were carried out in triplicate.

Antibody competition assays were carried out by first loading the HA molecule onto the probe for 300 s, followed by binding the competing antibodies (39.29, 5J8 or F005-126) for 300 s. These loaded HA-IgG complexes were then allowed to bind to H1 + H3 CR antibodies (D1 H1-3/H3-3 and D1 H1-17/H3-14) for 300 s. Competition was determined by comparison of H1 + H3 CR antibody binding to uncomplexed HA molecules. Data analysis was carried out using Octet software, version 8.0.

**Production of pseudotyped lentiviral vectors and measurement of neutralizing activity of monoclonal antibodies.** Influenza pseudotyped lentiviral vectors expressing a luciferase reporter gene were produced as described<sup>51</sup>. Briefly, the following plasmids: 17.5 µg of pCMVΔR8.2, 17.5 µg of pHR<sup>+</sup>CMV-Luc, 60 ng of pCMV Sport/h TMPRSS2, 1 µg CMV/R-HA and 0.125 µg of corresponding CMV/R-NA of a given strain of influenza virus, were transiently cotransfected into 293T cells by use of Eugene6 (Promega). Cells were transfected overnight and replenished with fresh medium. 48 h later, supernatants were harvested, filtered through a 0.45-µm PES membrane filter, aliquoted, and frozen at -80 °C.

For neutralization assays, recombinantly expressed monoclonal antibodies at various dilutions were mixed with 50 µl of pseudoviruses and then added to 293A cells in 96-well plates (10,000 cells per well). 48 h later, cells were lysed in cell culture lysis buffer (Promega, Madison, WI) before mixing with luciferase assay reagent (Promega). Light intensity was quantified with a Perkin Elmer microplate reader, and antibody neutralization resulted in lower light intensity.

**Hemagglutination inhibition (HAI) assay.** The HAI assay was used to assess the abilities of functional antibodies specific for HA to inhibit agglutination of turkey erythrocytes. The protocol was adapted from the CDC laboratory-based influenza surveillance manual<sup>52</sup>. To inactivate nonspecific inhibitors, sera were treated with Receptor Destroying Enzyme (RDE; Denka Seiken, Co., Japan) prior to being tested<sup>53</sup>. Briefly, three parts RDE was added to one part serum and incubated overnight at 37 °C. RDE was inactivated by incubation at 56 °C for ~30 min. RDE-treated sera, or recombinantly expressed monoclonal antibodies, were two-fold serially diluted in v-bottom microtiter plates. An equal volume of each influenza virus strain (A/California/07/2009, A/Perth/16/2009 or B/Brisbane/60/2008), adjusted to approximately 8 HAU per 50 µl, was added to each well. The plates were covered and incubated at room temperature (RT) for 20 min followed by the addition of 1% turkey erythrocytes (RBC; Lampire Biologicals, Pipersville, PA, USA) in PBS. Red blood cells were stored at 4 °C and used within 72 h of preparation. The plates were mixed by agitation, covered and the RBCs were allowed to settle for 1 h at RT. The HAI titer was determined

by the reciprocal dilution of the last well that contained nonagglutinated RBC. Positive and negative serum controls were included for each plate.

**Plaque-reduction assay.** Monolayers of MDCK cells in 6-well plates were infected with 100 plaque-forming units (p.f.u.) of influenza virus in 100 µl of Dulbecco's modified Eagle's medium (DMEM) in presence or absence of the tested monoclonal antibodies and incubated for 1 h at 37 °C. The inoculum was removed from the cells, and the cells were washed with PBS buffer. DMEM supplemented with 1% agar and 1 µg/ml TPCK-trypsin was added to each well. After 48 h of incubation at 37 °C, the cells were fixed with 4% formaldehyde, the agar plugs were removed and the cells were stained with 0.1% crystal violet to estimate the titer of virus in the presence or absence of the neutralizing antibodies. Concentration of tested antibodies with 50% of viral titer reduction is considered as IC<sub>50</sub> (µg/ml), performed in three independent experiments.

**Testing of binding of H1 + H3 cross-reactive antibodies to infected cells using flow cytometry.** MDCK cells plated in 6-well plate format (approximately  $9 \times 10^5$  cells/well) were infected with pandemic H1N1 strain A/Netherlands/602/09 (NL09) at a multiplicity of infection (MOI) of 1. They were incubated for 17 h at 37 °C before being trypsinized and fixed with 70% ethanol. Tested monoclonal antibodies were added at 5 µg/ml, incubated for 1 h and detected with 1:1,000 diluted Alexa-Fluor-488-conjugated goat anti-human-IgG (Life Technologies; A11013) using flow cytometry.

**IgG passive transfer and therapeutic protection to influenza virus challenge in mouse model.** For passive transfer experiments, mice were randomized into groups of five, and animal groups were not blinded to the investigators. Sample size was based on previous experience with similar experimental set-ups for antibody passive transfer influenza virus challenge experiments that used the same virus strains and challenge doses. Female 6- to 8-week-old BALB/c mice ( $n = 5$  per group) were intraperitoneally injected with monoclonal antibodies diluted in PBS. Two hours after transfer mice were anesthetized with a ketamine/xylazine mixture (0.15 mg/kg and 0.03 mg/kg) and intranasally infected with ten murine lethal doses of the respective challenge virus in 50 µl of PBS. Weight loss and survival were monitored over a period of 14 d, and animals that crossed the humane end point of 75% of the initial body weight were euthanized. Initially, monoclonal antibodies D1 H1-1/H3-1, D1 H1-9/H3-7, D1 H1-3/H3-3, D1 H1-17/H3-14 and D2 H1-1/H3-1 were tested at 5 mg/kg for protection against the pandemic H1N1 strain A/Netherlands/602/09 (NL09). D1 H1-3/H3-3, D1 H1-17/H3-14 and D2 H1-1/H3-1 were also tested at lower doses (1 mg/kg and 0.5 mg/kg) against NL09. The protective breadth of these three mAbs was tested at 5 mg/kg against H3N2 strain X-31 (HA and NA from A/Hong Kong/1/68 and backbone of A/PR/8/34). The lung viral titers of mice ( $n = 3$  per group) that were prophylactically treated with D1 H1-3/H3-3 and D1 H1-17/H3-14 2 h before an infection with NL09 were analyzed. Lungs were harvested on day 3 and day 6 after infection, homogenized and used for plaque assays.

In therapeutic-setting protection experiments, female 6- to 8-week-old BALB/c mice ( $n = 10$  per group) were challenged first with NL09 and then received D1 H1-3/H3-3 and D1 H1-17/H3-14 monoclonal antibodies diluted in PBS, 24 and 48 h post infection (h.p.i.) at 5 mg/kg.

In all cases, irrelevant human IgG1 was used as negative control and bNAb CR9114 served as positive control. All animal experiments complied with the guidelines and protocols approved by the Icahn School of Medicine at Mount Sinai Institutional Animal Care and Use Committee.

**Electron microscopy and single-particle analysis.** For the initial analysis and screening of HA-Fab mixtures, protein samples diluted to approximately 0.05 mg/ml were adsorbed to glow-discharged carbon-coated copper grids, washed with several drops of buffer containing 20 mM HEPES, pH 7.0, and 150 mM NaCl and negatively stained with 0.75% uranyl formate, pH 5.0. Micrographs were recorded at a magnification of 100,000× on a FEI Tecnai T20 microscope operated at 200 kV and equipped with a 2 k × 2 k Eagle CCD camera. The pixel size was 2.22 Å/pixel. SerialEM<sup>54</sup> was used for data collection. Particles were picked using EMAN2.1 (ref. 55) automatically or manually. Particle alignment and reference-free classification were carried out in EMAN2 and SPIDER<sup>56</sup>.



The initial analysis revealed that a subset of HA–Fab combinations contained highly heterogeneous mixtures of aggregates, free HA trimers and Fab fragments, partially unfolded HA trimers and dimers with varying numbers of Fab fragments bound, HA dimers and monomers, and, as a major component, the complex between a monomer of HA and a single Fab fragment (**Supplementary Fig. 10a**). Analysis of a dataset containing approximately 12,000 particles revealed that the latter complex was represented by about 50% of all particles and had a strong preferential orientation, with well-defined Fab fragments and head moieties of the HA and less well-defined membrane proximal regions ('tails'). The random conical tilt (RCT) approach<sup>57</sup> was utilized to obtain the three-dimensional map of the complex. Grids were prepared as described above, except that the sample was supplemented with tobacco mosaic virus to simplify alignment of untilted and tilted micrographs. To accelerate data collection,  $5 \times 5$  to  $7 \times 7$  montages of untilted and  $45^\circ$ -tilted images from same areas of the grid were obtained using SerialEM. All further analyses were performed with SPIDER. Montages were aligned automatically, and pairs of untilted and tilted images were formed using a custom written script. 4,843 pairs of particles consistent in size with the HA monomer/single Fab complex were picked and centered manually with JWeb<sup>56</sup>. Reference-free classification of the particles from untilted micrographs windowed into  $128 \times 128$  boxes into 20 classes revealed that at least 3,351 of them (nine classes) represented the complex (**Supplementary Fig. 10b**). The tilted particles corresponding to each 2D class were grouped, rotationally aligned and used to compute three-dimensional reconstructions, which were then inspected in UCSF Chimera<sup>58</sup>, aligned and merged. The resulting map was subjected to translational refinement, yielding the RCT map of the complex (**Supplementary Fig. 10c**). This map was then used as the initial model for three-dimensional reconstruction and refinement using reference projections<sup>59</sup>. Particles from both the untilted and tilted micrographs were used for the refinement. No contrast transfer function (CTF) correction was performed. The 'resolution' (level of self-consistency) of the final map was 22 Å when a Fourier shell correlation (FSC) threshold of 0.5 was used. Forward projections of the map corresponded well to two-dimensional classes (**Supplementary Fig. 10d**). The level of the map was chosen based on fitting a Fab domain into the corresponding density. The map was visualized in UCSF Chimera.

**Statistical analysis.** Statistical analyses were performed using GraphPad Prism 5.0 (GraphPad Software, Inc., San Diego, CA), unless specifically noted otherwise in the figure legends. All of the statistical tests performed are described in the figure legends, and correlations were considered significant at  $P < 0.05$ .

**Data availability.** The proteomics data reported in this paper are tabulated in **Supplementary Data 1–3** and are archived through MassIVE (<http://massive.ucsd.edu>).

49. McDaniel, J.R., DeKosky, B.J., Tanno, H., Ellington, A.D. & Georgiou, G. Ultra-high-throughput sequencing of the immune receptor repertoire from millions of lymphocytes. *Nat. Protoc.* **11**, 429–442 (2016).
50. Cox, J., Michalski, A. & Mann, M. Software lock mass by two-dimensional minimization of peptide mass errors. *J. Am. Soc. Mass Spectrom.* **22**, 1373–1380 (2011).
51. Yang, Z.Y. *et al.* Selective modification of variable loops alters tropism and enhances immunogenicity of human immunodeficiency virus type 1 envelope. *J. Virol.* **78**, 4029–4036 (2004).
52. Gillim-Ross, L. & Subbarao, K. Emerging respiratory viruses: challenges and vaccine strategies. *Clin. Microbiol. Rev.* **19**, 614–636 (2006).
53. Ross, T.M., Xu, Y., Bright, R.A. & Robinson, H.L. C3d enhancement of antibodies to hemagglutinin accelerates protection against influenza virus challenge. *Nat. Immunol.* **1**, 127–131 (2000).
54. Mastronarde, D.N. Automated electron microscope tomography using robust prediction of specimen movements. *J. Structural Biology* **152**, 36–51 (2005).
55. Tang, G. *et al.* EMAN2: An extensible image processing suite for electron microscopy. *Journal of Struct. Biol.* **157**, 38–46 (2007).
56. Frank, J. *et al.* SPIDER and WEB: processing and visualization of images in 3d electron microscopy and related fields. *J. Struct. Biol.* **116**, 190–199 (1996).
57. Radermacher, M., Wagenknecht, T., Verschoor, A. & Frank, J. Three-dimensional reconstruction from a single-exposure, random conical tilt series applied to the 50S ribosomal subunit of *Escherichia coli*. *J. Microsc.* **146**, 113–136 (1987).
58. Pettersen, E.F. *et al.* UCSF Chimera—a visualization system for exploratory research and analysis. *J. Comput. Chem.* **25**, 1605–1612 (2004).
59. Shaikh, T.R. *et al.* SPIDER image processing for single-particle reconstruction of biological macromolecules from electron micrographs. *Nat. Protoc.* **3**, 1941–1974 (2008).